Trigeminal nerve microstructure is linked with neuroinflammation and brainstem activity in migraine

Sarasa Tohyama,[1,2,†] Michael Datko,[1,2,3,†] Ludovica Brusaferri,[1,4,†] Lillian D. Kinder,[1,2,3] Jack H. Schnieders,[1] Mackenzie Hyman,[1] Alison M. Goldstein,[1,2] Melaina D. Gilbert,[1,2] Hope Housman,[1] Vi Le,[1,5] Kassandra Round,[1,2,3] Frances Marin,[3] Megan R. Heffernan,[1,5] Ronald G. Garcia,[6,7] Randy L. Gollub,[1,6] Robert R. Edwards,[8] Bruce R. Rosen,[1] Nouchine Hadjikhani,[1] Hsinlin T. Cheng,[5] Zev Schuman-Olivier,[3] Marco L. Loggia[1,9,‡] and Vitaly Napadow[1,2,8,‡]

[†,‡]**These authors contributed equally to this work.**

Abstract

Although the pathophysiology of migraine involves a complex ensemble of peripheral and central nervous system changes that remain incompletely understood, the activation and sensitization of the trigeminovascular system is believed to play a major role. However, non-invasive, *in vivo* neuroimaging studies investigating the underlying neural mechanisms of trigeminal system abnormalities in human migraine patients are limited.

Here, we studied 60 patients with migraine (55 females, mean age ± SD: 36.28 ± 11.95 years) and 20 age-/sex-matched healthy controls (19 females, mean age ± SD: 35.45 ± 13.30 years) using ultra-high field 7 Tesla diffusion tensor imaging and functional MRI, as well as PET with the translocator protein ligand [^{11}C]-PBR28. We evaluated MRI diffusivity measures and PET signal at the trigeminal nerve root, as well as brainstem functional MRI response to innocuous, ophthalmic trigeminal nerve territory stimulation.

Patients with migraine demonstrated altered white matter microstructure at the trigeminal nerve root (n=53), including reduced fractional anisotropy, compared to healthy controls (n=18). Furthermore, in patients, lower fractional anisotropy was accompanied by 1) higher neuroinflammation (i.e. elevated [^{11}C]-PBR28 PET signal) at the nerve root (n=36) and 2) lower

functional MRI activation in an ipsilateral pontine cluster consistent with spinal trigeminal nucleus (n=51). These findings were more robust on the right side, which was consistent with the observation that right headache dominant patients demonstrated higher migraine severity compared to left headache dominant patients in our cohort.

Multimodal imaging of the integrated neural mechanisms that characterize migraine underscores the importance of trigeminal system remodeling as both a key aspect of the dynamics underlying migraine pathophysiology and a target for therapeutic interventions.

Author affiliations:

1 Athinoula A. Martinos Center for Biomedical Imaging, Department of Radiology, Massachusetts General Hospital, Harvard Medical School, Boston, MA 02129, USA

2 Department of Physical Medicine and Rehabilitation, Spaulding Rehabilitation Hospital, Harvard Medical School, Boston, MA 02129, USA

3 Center for Mindfulness and Compassion, Department of Psychiatry, Cambridge Health Alliance, Harvard Medical School, Cambridge, MA 02141, USA

4 Department of Computer Science and Informatics, London South Bank University, London SE1 0AA, UK

5 Department of Neurology, Massachusetts General Hospital, Harvard Medical School, Boston, MA 02114, USA

6 Department of Psychiatry, Massachusetts General Hospital, Harvard Medical School, Boston, MA 02114, USA

7 School of Medicine, Universidad de Santander, Bucaramanga 680006, Colombia

8 Department of Anesthesiology, Perioperative and Pain Medicine, Brigham and Women's Hospital, Harvard Medical School, Boston, MA 02115, USA

9 Department of Anesthesia, Critical Care and Pain Medicine, Massachusetts General Hospital, Harvard Medical School, Boston, MA 02114, USA

Correspondence to:Vitaly Napadow, PhD, LAc

Spaulding Rehabilitation Hospital

300 First Ave, Suite 2150

Charlestown, MA 02129, USA

E-mail: VITALY@mgh.harvard.edu

Running title: Trigeminal microstructure in migraine

Keywords: migraine; trigeminal nerve; spinal trigeminal nucleus; DTI; PET; fMRI

Introduction

Migraine is a highly prevalent and disabling neurological condition[1], characterized by recurrent attacks of pulsating headache along the ophthalmic branch (V1) of the trigeminal nerve.[2] While the pathophysiology of migraine involves a complex ensemble of peripheral and central nervous system changes that remain incompletely understood, the activation and sensitization of the trigeminovascular system is believed to play a major role.[3] The trigeminovascular theory proposes that the onset of migraine attacks depends on the activation and sensitization of nociceptive sensory afferent fibers of the trigeminal nerve that densely innervate the cranial meninges and meningeal blood vessels.[4–7] Non-invasive, *in vivo* neuroimaging holds promise to further elucidate migraine mechanisms[8], and in particular, the involvement of the trigeminal system in migraine pathophysiology. However, employing advanced neuroimaging to study the trigeminal system has been difficult to accomplish because of the small-scale structure of the nerve and brainstem nuclei. Technical innovations with ultra-high field 7T MRI have significantly improved signal-to-noise ratio (SNR) and spatial resolution, thereby enhancing the investigation of peripheral nerves and the brainstem with both structural and functional MRI.[9–11]

Among the different MRI techniques available, diffusion tensor imaging (DTI) measures the three-dimensional movement of water molecules in biological tissue to characterize white matter microstructure.[12] For quantitative assessment, DTI metrics, such as fractional anisotropy (FA), radial diffusivity (RD), mean diffusivity (MD) and axial diffusivity (AD), can be computed. Significant advances in DTI techniques have elucidated underlying neural mechanisms and

pathophysiology in various neurological disorders[13–17], including migraine.[18–24] However, very few DTI studies have specifically probed the trigeminal nerve and brainstem trigeminal nuclei in migraine patients. These studies identified reduced FA at the root entry zone (REZ) of the trigeminal nerve (also known as the motor/sensory root or trigeminal root)[25] and increased MD in the area of the spinal trigeminal nucleus (SpV).[26] No studies to date have employed ultra-high field 7T MRI to more precisely investigate trigeminal system abnormalities in migraine patients.

Importantly, no studies have examined the structure-function associations of the trigeminal system by combining structural MRI (i.e. DTI) with measures of neuroimmune activation using PET or measures of functional activation using functional MRI (fMRI). Employing the methodology of integrated (i.e. simultaneous) PET/MRI with the [^{11}C]-PBR28 radioligand, we recently demonstrated elevated levels of the 18-kDa translocator protein (TSPO; a putative marker of glial and macrophage activation and/or density)[27–29] in migraine patients with aura, in brain areas involved with nociceptive processing[30] as well as the parameningeal tissues.[31] However, whether neuroinflammation also impacts the trigeminal nerve in migraine patients remains entirely unknown. Furthermore, while numerous fMRI studies in migraine patients have localized brain areas implicated in the multidimensional experience of pain (most notably SpV) and visual processing through various phases of the migraine cycle[5,32–37], the linkage between microstructural alterations and neuroinflammation of the trigeminal nerve, as well as brainstem functional activity has yet to be explored.

Therefore, a multimodal neuroimaging approach to study the trigeminal system in migraine patients may provide insight into the unique interplay of trigeminal microstructural alterations, inflammation, and functional activity, for this complex and difficult-to-treat disorder. Hence, in this study, we employed (1) 7T DTI to investigate white matter microstructural alterations of the trigeminal nerve, (2) [^{11}C]-PBR28 PET to investigate neuroinflammation of the trigeminal nerve, and (3) 7T fMRI to explore brainstem (e.g. trigeminal nucleus) activation to trigeminal sensory stimulation in patients with migraine. Specifically, we hypothesized that migraine patients will demonstrate (1) altered white matter microstructure at the trigeminal REZ, characterized by lower FA, compared with healthy controls, and that (2) these alterations will be linked with elevated PET signal (i.e. neuroinflammation) in the same anatomical region and reduced SpV fMRI response to innocuous, ophthalmic trigeminal nerve territory stimulation.

Materials and methods

Participant characteristics, screening, and clinical measures

This study enrolled patients with migraine based on the following criteria: (1) diagnosis of either migraine without aura or migraine with aura according to the third edition of the International Classification of Headache Disorders (ICHD-3)[2] and (2) 4–20 migraine headache days per month determined based on the completion of at least 75% of electronic daily headache diaries in a 4-week time frame following written informed consent. While episodic migraine was the target population, headache frequency up to 20 days per month was included, as month-to-month headache frequency variability is often seen in migraine patients.[38] This criterion has been used in prior studies that also included both episodic and chronic migraine patients.[39] Furthermore, if a patient reported >15 headaches, the diaries (which included medication usage) were evaluated by a neurologist (H.T.C.) and patients with medication-overuse headaches were excluded. On each daily headache diary, participants were asked to report whether they had a headache that day. If yes, they were prompted to rate pain intensity (rated on a numerical rating scale (NRS) of 0–10; 0: no pain, 10: worst pain imaginable) and to state whether the headache was lateralized to one side (categorized as right, left, or both). Participants were also asked questions regarding symptoms related to nausea, photophobia, and phonophobia. Participants continued to complete daily diaries throughout the study trial and these data were used to assess clinical characteristics, including number of headache days, dominant headache side, and mean pain intensity. Healthy control participants also underwent the same screening procedure and 4-week period of daily diaries, and were excluded based on the following criteria: (1) any first degree relative with a history of migraine, (2) experienced any headache characteristic of migraine, (3) any personal history of major neurological or psychiatric conditions, or (4) any MRI contraindications. Criteria (3) and (4) were also exclusionary criteria for migraine patients. All study procedures were approved by the Massachusetts General Brigham Institutional Review Board and were part of an ongoing clinical trial evaluating the effects of mind-body interventions on the brain circuitry in migraine (ClinicalTrials.gov # NCT03592329). All participants provided written informed consent according to the Declaration of Helsinki prior to the study.

Overall, a total of 80 participants, 60 patients with migraine (55 females, mean age ± SD: 36.28 ± 11.95 years, 54 episodic and 6 chronic) and 20 age-/sex-matched healthy controls (19 females, mean age ± SD: 35.45 ± 13.30 years) were enrolled to complete two baseline neuroimaging sessions (7T MRI and 3T PET/MRI), separated by a maximum of 3 weeks, at the Martinos Center for Biomedical Imaging in Boston, Massachusetts. Information regarding the total sample size for participant enrollment and completion across imaging modalities is provided in **Supplementary Figure 1**. All imaging data analyzed herein were collected from the baseline neuroimaging sessions before exposure to an 8-week mind-body intervention.

7T MRI acquisition

All participants underwent an MRI session using a 7T scanner (MAGNETOM Terra, Siemens Healthineers, Erlangen, Germany) equipped with a custom-built 64-channel head coil.[40] T1-weighted anatomical data were collected with the following parameters: 3D MP-RAGE pulse sequence, voxel size = 0.8 x 0.8 x 0.8 mm^3, repetition time (TR) = 2530 ms, echo time (TE) = 1.65 ms, flip angle = 7°, field of view (FOV) = 240 mm, GRAPPA acceleration factor = 2. Brainstem-focused diffusion-weighted imaging (DWI) data were collected with the following parameters: spin-echo echo-planar imaging (EPI) sequence, voxel size = 1 x 1 x 1 mm^3, 64 directions, 4 interleaved B_0, b = 1000 s/mm^2, TR = 5900 ms, TE = 68 ms, 1 excitation, GRAPPA acceleration factor = 3, matrix = 192 x 192, flip angle = 90°, FOV = 192 mm, 52 axial slices centered on the brainstem and tilted parallel to the AC-PC (anterior commissure-posterior commissure), echo spacing = 0.81 ms, total acquisition time = 7.68 minutes. Additionally, two baseline images with b = 0 s/mm^2 were collected in the forward and reverse phase encoding directions (anterior/posterior), respectively, for susceptibility-induced distortion correction. Whole-brain fMRI data were collected with the following parameters: simultaneous multi-slice EPI sequence, acceleration factor = 4, voxel size = 1.5 x 1.5 x 1.5 mm^3, TR = 1190 ms, TE = 22 ms, flip angle = 60°, FOV = 192 mm, 92 axial slices with no gap prescribed parallel to the AC-PC, 326 volumes, total acquisition time = 7.25 minutes.

Electrical forehead stimulation fMRI

For the fMRI scan, electrical forehead stimulation targeting the ophthalmic trigeminal nerve territory was applied to investigate brainstem fMRI response to trigeminal sensory afference. Specifically, non-painful stimulation was delivered on the right side of the forehead via a direct-current stimulation device (UROstim, Schwa-medico, Ehringshausen, Germany) with a 5 Hz pulse train, a pulse width of 450 μs, at an amplitude of 7 mA (stimulus-matched across participants). A block fMRI design was used (ON: 8 s, OFF: 14 s, 17 repetitions). The right side was chosen for consistency with prior studies that used right-sided stimulation to examine fMRI response to trigeminal sensory stimulation.[32,33] Before fMRI, participants rated the intensity of the stimulation using a NRS of 0 to 10 (0: no sensation, 10: pain sensory threshold, i.e. on the verge of painful sensation). Unless rated as imperceptible or above pain threshold, the current was set at 7 mA for the fMRI scan. Participants were instructed to keep their eyes open and focused on a central fixation cross, pay attention to the forehead stimulation as it turns on and off, and remain still in a supine position.

3T PET/MRI acquisition

During an initial screening visit, participants were consented and genotyped for the Ala147Thr polymorphism in the TSPO gene, which affects the binding affinity for several TSPO radioligands, including [^{11}C]-PBR28.[41] Only participants with the Ala/Ala or Ala/Thr genotypes (high- and mixed-affinity binders, respectively) were included in the study, and genotype was used as a covariate in the statistical analysis. Participants with the Thr/Thr genotype (low-affinity binders) were excluded and are not represented in our dataset.

Dynamic PET/MRI scans were conducted using a 3T Tim Trio whole-body MRI with a dedicated brain PET insert (BrainPET)[42], with a spatial resolution of 2–3 mm.[43] Participants received an intravenous bolus injection of up to ~15 millicuries (mCi) of [^{11}C]-PBR28.[44] PET imaging acquisitions were performed as detailed in previous studies.[45,46] Structural T1-weighted images were acquired for anatomical localization, spatial normalization of PET data, and the generation of attenuation correction maps with the following parameters: a 3D MP-RAGE pulse sequence,

voxel size = 1 x 1 x 1 mm^3, TR = 2530 ms, TE = 1.63 ms, flip angle = 7°, FOV = 280 mm, GRAPPA acceleration factor = 2.

Neuroimaging data processing

All MRI data were organized using Brain Imaging Data Structure (BIDS), a standard format for structuring neuroimaging data.[47] For DWI, all postprocessing steps were performed in FSL 6.0.1.[48] The two pairs of baseline images acquired in the forward and reverse phase encoding directions were used to estimate and correct susceptibility-induced distortions using TOPUP.[49] After removal of non-brain voxels using BET, eddy current-induced distortions and subject movements were corrected using EDDY.[50,51] DTIFIT was used to fit a diffusion tensor model at each voxel and generate DTI metric maps of FA, RD, MD, and AD.[52] After quality control of the data, nine participants (seven patients and two healthy controls) were excluded from DTI data analyses due to the images showing significant warping and distortions, and therefore poor visualization of the trigeminal REZ.

For PET, the data were corrected for scatter and attenuation using in-house tools developed at the Martinos Center for Biomedical Imaging.[53] Quality control of the data was performed visually to ensure the absence of artifacts, including excessive motion. Then, 30-minute static standardized uptake value (SUV) PET images were reconstructed from data collected between ~60-90 minutes post-injection. These images were co-registered to the structural T1-weighted images (for localization of the trigeminal nerve REZ), and then smoothed with a 5 mm full width at half maximum (FWHM) Gaussian kernel to improve the SNR while minimizing signal spillover. Finally, SUV ratio (SUVR) values were obtained using whole-brain normalization as previously described.[54] One healthy control participant was excluded from the PET analyses due to poor visualization of the trigeminal REZ.

For fMRI, first, due to the field inhomogeneities that are especially pronounced at 7T, the T1-weighted images were intensity bias corrected using SPM12[55] as described by Zaretskaya *et al.*[56] The bias field corrected T1-weighted images and fMRI images were then preprocessed using *fMRIPrep* 20.1.1.[57] As part of *fMRIPrep*, several confounding time-series were also calculated,

including framewise displacement (FD) and head-motion estimates (i.e. the six rigid-body motion parameters). Quality control of the data was performed, including visual inspection of image artifacts, assessment of significant head motion, and co-registration success. Significant head motion was quantified based on a criterion of mean FD > 0.5 mm (i.e. participants were excluded if they had a mean FD value greater than 0.5 mm). All participants were below this threshold. We then examined the maximum FD and excluded four participants (two patients and two healthy controls) with a maximum FD value greater than 3 mm (i.e. twice the fMRI voxel size) and/or 2 standard deviations greater than the mean.

Neuroimaging data analyses

For the DTI analyses, the FA map in individual space was used to visualize the trigeminal nerves in the axial view using 3D Slicer 4.6.2.[58] Regions-of-interest (ROI) were then placed at the REZ of the right and left trigeminal nerve for extraction of DTI metrics (FA, RD, MD, and AD) (**Fig. 1A**). The small isotropic voxel size of 1 x 1 x 1 mm^3 allowed for individual level tailoring of ROI placement and volume. Specifically, all ROIs were 2 voxels in volume in both the x- and y-dimension, while the number of voxels in the z-dimension varied from 1–3 depending on each individual's nerve root geometry. Following extraction of DTI metrics, statistical analyses were performed. Differences in DTI metrics between groups were assessed using independent-samples t-tests. Associations between DTI metrics and clinical measures were assessed using Pearson's correlations. Normality of the data was assessed using the Shapiro-Wilk test and non-parametric equivalent tests were performed for any non-normally distributed variables. False discovery rate correction was used to correct for multiple comparisons for the four DTI metrics. All statistical analyses in this study were conducted using a combination of SPSS 28.0 (IBM, Armonk, NY) and R/RStudio (R 4.3.1, RStudio 2023.09.0), with statistical significance set at $p < 0.05$ or $q < 0.05$ (multiple comparison corrected p-value).

For the PET analyses, the structural T1-weighted image in PET space was used to visualize the trigeminal nerves given the coarser PET resolution (2–3 mm). The same manual ROI placement approach was used as the DTI dataset described above on the co-registered T1-weighted image. Of note, one author (S.T.) with expertise in clinical neuroimaging and trigeminal nerve anatomy

placed all ROIs in both the DTI and PET images for consistency and uniformity across imaging modalities, and an additional trained rater performed a quality control assessment to ensure accurate ROI placement. The mean SUVR value within the right and left trigeminal REZ was calculated in individual space for each participant. Following extraction of SUVR values, we conducted a partial correlation analysis (i.e. controlling for TSPO genotype) within the migraine patient group only to assess a possible link between reductions in white matter microstructural integrity, measured by FA, and neuroinflammation, measured by [^{11}C]-PBR28 SUVR. This analysis was performed for both the right and left trigeminal REZ. Additionally, we performed this analysis by computing 'left–right' difference scores for both FA and the PET signal (i.e. ΔFA and Δ[^{11}C]-PBR28 SUVR), in order to subtract out and thus minimize the confounding effects of factors affecting PET signal globally (e.g. individual differences in ligand metabolism)[59], which may hamper our ability to detect the association between true neuroinflammatory signal and FA. Next, we tested the hypothesis that trigeminal nerve inflammation will be detected in patients with reduced trigeminal nerve microstructural integrity (i.e. the low FA patients), but not in those with normal FA. To this end, we first split the migraine patient group into two subgroups – high FA (MIG_{HighFA}) and low FA (MIG_{LowFA}) – defined by FA values greater or less than the lowest FA value in the healthy control group. This cutoff threshold was pragmatically defined to identify patients that are truly different from the normal healthy control range. Then, we performed a one-way ANCOVA to assess PET signal differences across the three groups (MIG_{HighFA}, MIG_{LowFA}, and healthy controls), accounting for genotype as a covariate. Statistically significant group effects were further decomposed using the Dunnett's post-hoc test, to compare each patient subgroup against a single healthy control group. This analysis was conducted for both the right and left side.

Given our interest in imaging the brainstem trigeminal system, including the pontine nuclei, the fMRI analyses entailed a pipeline specifically probing brainstem fMRI response to trigeminal sensory afference. A brainstem mask in ICBM152 MNI space previously used and described by Sclocco *et al.*[10] was implemented by transforming this mask into individual functional spaces using Advanced Normalization Tools (ANTs) 2.3.5.[60] The masking step resulted in fMRI voxels spatially restricted to the brainstem, which aided removal of surface vessel cardiogenic noise prior to spatial smoothing. Subsequently, first-level General Linear Model (GLM) analyses were performed within the specified mask using FEAT in FSL.[61] A single explanatory variable (EV) was defined with a custom text file specifying the forehead stimulation block design (i.e. stimulus

onset and duration), convolved with the canonical hemodynamic response function (Double-Gamma). The six head-motion parameters of each participant calculated as part of *fMRIPrep* were included as additional confound EVs. Spatial smoothing with a 3 mm FWHM Gaussian kernel and temporal filtering with a high pass cutoff of 50 s were applied. The outputs of this first-level analysis (i.e. the contrast of parameter estimates and its variance) were transformed into standard MNI152 space and fed into group-level FEAT analyses using FMRIB's Local Analysis of Mixed Effects (FLAME 1+2) (uncorrected $p < 0.05$).[62] We used uncorrected thresholds, as in previous brainstem fMRI studies, due to the reduced SNR and very small nuclei that characterize the brainstem compared to cortical responses.[10] A single-group average GLM analysis was performed to yield an fMRI activation map of brainstem response to trigeminal sensory afference. In addition, to explore structure-function associations, FA of the right trigeminal nerve REZ in each migraine patient was added as a covariate to the fMRI GLM. The right REZ FA was chosen because the fMRI task involved stimulating the trigeminal nerve territory on the right (ipsilateral) side of the forehead. Lastly, a group brainstem fMRI response contrast was performed between migraine patients and healthy controls (also uncorrected $p < 0.05$).

Migraine headache laterality and pain severity

To explore the association of imaging findings with migraine symptom severity and laterality, we examined clinical data from the daily headache diaries collected within a 30-day window prior to each patient's 7T MRI and PET/MRI visits, respectively. Headache laterality was examined by computing the number of days participants reported a headache on either the right, left, or both sides. Participants were defined as right-dominant or left-dominant based on the highest frequency of headaches reported on either side. Headaches reported on both sides were not considered for this analysis. Participants with a tie between the number of right and left sided headaches were categorized as "bilateral" and excluded from this analysis. Furthermore, we compared mean pain intensity (based on a NRS of 0–10 as describe above) between right headache dominant and left headache dominant patients using an independent-samples t-test. For this analysis, only headaches meeting criteria consistent with the ICHD-3 diagnostic criteria for migraine were included (inclusion criteria: two out of the following four – 1) unilateral location, 2) pulsating quality, 3)

pain intensity of at least 4 out of 10, and 4) movement makes headache worse; and at least one of the following – 1) nausea or vomiting and 2) sensitivity to light/sound).

Results

Altered white matter microstructure of the trigeminal nerve in migraine

Our brainstem-focused high-resolution 7T DWI acquisition successfully delineated the small-scale structure of the trigeminal REZ (**Fig. 1A**). A total of 53 migraine patients (50 females, mean age ± SD: 36.34 ± 11.90 years, 39 in the interictal phase and 14 in the ictal phase) and 18 healthy controls (17 females, mean age ± SD: 35.94 ± 14.01 years) were included in the DTI analyses. There were no significant differences in age ($t_{(69)} = 0.12$, $p = 0.91$) or sex ($\chi^2(1) = 2.78 \times 10^{-4}$, $p = 0.99$) between the 2 groups. Patients with migraine demonstrated significantly lower FA ($t_{(69)} = -6.04$, $p = 6.89 \times 10^{-8}$, $q = 2.76 \times 10^{-7}$), and higher RD ($U = 231$, $p = 0.0012$, $q = 0.0023$) and MD ($U = 308$, $p = 0.026$, $q = 0.034$), in the right trigeminal REZ compared to healthy controls. No significant differences were observed in AD ($U = 404$, $p = 0.34$, $q = 0.34$) (**Fig. 1B**). Migraine patients also demonstrated significantly lower FA ($t_{(69)} = -3.13$, $p = 0.0026$, $q = 0.010$) in the left trigeminal REZ compared to healthy controls, however, no significant differences were observed in RD ($U = 321$, $p = 0.039$, $q = 0.078$), MD ($U = 356$, $p = 0.11$, $q = 0.15$), or AD ($t_{(69)} = 0.42$, $p = 0.67$, $q = 0.67$) (**Fig. 1C**). No significant differences were found in ROI volume (i.e. number of voxels) between migraine patients and healthy controls on the right ($t_{(69)} = -0.97$, $p = 0.34$) and left side ($t_{(69)} = -0.12$, $p = 0.91$). Furthermore, no significant associations were found between FA (the most robust DTI metric) and clinical variables, such as number of headache days and mean headache pain intensity in the 30 days prior to the 7T MRI date, or migraine disease duration, for the right and left side, separately ($p > 0.50$ for all correlations).

Association between trigeminal nerve microstructural alterations and neuroinflammation

A subset of 36 migraine patients (31 in the interictal phase and 5 in the ictal phase) and 10 healthy controls with both DTI and PET images were included in the PET analyses. Our dynamic PET acquisition successfully localized the PET signal at the level of the trigeminal REZ (**Fig. 2A**). The correlations between trigeminal nerve REZ FA and [^{11}C]-PBR28 PET signal revealed an overall negative relationship. Specifically, we observed a statistically significant negative correlation between FA and PET signal in the right trigeminal REZ (r = -0.45, p = 0.0063, 95% CI: [-0.68, -0.14]), while the left trigeminal REZ did not reach significance (r = -0.24, p = 0.17, 95% CI: [-0.53, 0.10]). Intriguingly, the correlation was even stronger when testing 'left–right' difference scores (i.e. ΔFA versus ΔPET signal) (r = -0.59, p = 0.00020, 95% CI: [-0.77, -0.32]) (**Fig. 2B**).

The ANCOVA analysis, comparing the PET signal between migraine patients split based on FA values (i.e. MIG_{HighFA} and MIG_{LowFA}) and healthy control groups, revealed a statistically significant group effect in the right trigeminal REZ (p = 0.0029). Post-hoc analyses using the Dunnett's test indicated that this effect was driven by patients in the MIG_{LowFA} group, which showed elevated PET signal compared to healthy controls (p = 0.0095), whereas the MIG_{HighFA} group did not (p = 0.72). For the left trigeminal REZ, the group effect did not reach significance (p = 0.21) (**Fig. 2C**).

Brainstem response to trigeminal sensory afference and its association with nerve microstructure

A total of 58 migraine patients (43 in the interictal phase and 15 in the ictal phase) and 18 healthy controls were included in the fMRI analyses. All participants tolerated the electrical forehead stimulation fMRI protocol (**Fig. 3A**) and rated the stimulus as moderately intense but non-painful (mean sensory rating before fMRI ± SD = 4.51 ± 0.90, mode stimulus intensity = 7 mA). There were no significant differences between migraine patients and healthy controls in stimulation intensity (mean intensity ± $SD_{patients}$ = 7.91 ± 1.25 mA, mean intensity ± $SD_{controls}$ = 7.75 ± 0.97 mA; $t_{(74)}$ = 0.50, p = 0.62) or sensory rating (mean rating ± $SD_{patients}$ = 4.59 ± 0.85 mA, mean rating

$\pm$ $SD_{controls}$ = 4.25 $\pm$ 1.02 mA; $t_{(74)}$ = 1.40, p = 0.16). In response to stimulating the right side of the forehead, patients with migraine demonstrated brainstem activation in a cluster consistent with the right (ipsilateral) SpV. All brainstem fMRI clusters identified from this analysis are reported in **Supplementary Table 1**.[63] We also found a significant positive association between right trigeminal REZ FA and fMRI activation in the right SpV in a subset of 51 migraine patients with both DTI and fMRI images (β = 0.26, p < 0.05) (**Fig. 3B**). To aid visualization of SpV and comparison with the Duvernoy's brainstem atlas, we displayed the fMRI cluster over a high resolution (0.2 mm isotropic voxel size) *ex vivo* B_0 brainstem image, as previously described.[10,64] Based on this visualization and use of the Duvernoy's brainstem atlas, we estimate the fMRI cluster to be at the level of the pars oralis of SpV. Lastly, comparison of brainstem fMRI response between migraine patients (n=58) and healthy controls (n=18) revealed overall increased fMRI response in migraine patients across various brainstem nuclei, including the right SpV (**Supplementary Table 2**).

Influence of migraine headache laterality and pain severity on neuroimaging outcomes

Given the lateralization of some of our neuroimaging findings, we further explored clinical outcomes, including migraine headache laterality and pain severity. Specifically, given that the group differences in the PET signal, and its association with FA, were stronger on the right side, we tested the hypothesis that our participants had a preponderance of right-sided symptoms. Indeed, during the 30-day window prior to the PET/MRI visit, 15 migraine patients were categorized as right-side dominant for headaches, whereas only 11 were left-side dominant, and 9 reported predominantly bilateral symptoms. Additionally, 14 out of 15 right-side dominant patients (93.3%) reported headaches that met our criteria for migraine, whereas fewer left-sided dominant patients (7 out of 11, 63.6%) reported such headaches. Moreover, mean migraine pain intensity was significantly higher among right-dominant compared to left-dominant patients (mean pain intensity $\pm$ $SD_{right\text{-}dominant}$ = 5.53 $\pm$ 1.37, mean pain intensity $\pm$ $SD_{left\text{-}dominant}$ = 4.48 $\pm$ 0.68; $t_{(19)}$ = 2.34, p = 0.031).

Similar findings were noted for the 7T MRI visit. During the 30-day window prior, 22 migraine patients were categorized as right-side dominant for headaches, whereas only 16 were left-side dominant, and 13 reported predominantly bilateral symptoms. 21 out of 22 right-side dominant patients (95.5%) reported headaches that met our criteria for migraine, whereas fewer left-sided dominant patients (13 out of 16, 81.3%) reported such headaches. Mean migraine pain intensity differences did not reach significance between right- versus left-dominant patients, though a trend is noted (mean pain intensity ± $SD_{right\text{-}dominant}$ = 5.57 ± 1.57, mean pain intensity ± $SD_{left\text{-}dominant}$ = 4.83 ± 0.78; $t_{(31)} = 1.82$, $p = 0.078$). However, when the data were explored in a shorter, 15-day time window, we observed significantly higher mean migraine pain intensity among right-dominant compared to left-dominant patients (mean pain intensity ± $SD_{right\text{-}dominant}$ = 5.85 ± 1.79, mean pain intensity ± $SD_{left\text{-}dominant}$ = 4.56 ± 1.44; $t_{(24)} = 2.10$, $p = 0.046$).

Discussion

This study employed a multimodal neuroimaging approach, combining ultra-high field 7T DTI and fMRI, as well as integrated PET/MRI, to reveal both structural and functional alterations of the trigeminal system in migraine. Our key findings were that patients with migraine demonstrated altered white matter microstructure in the trigeminal nerve REZ, characterized principally by a reduction in the DTI measure of FA. These structural alterations were linked with elevated inflammation in the same anatomical region as measured by [^{11}C]-PBR28 PET and reduced fMRI response to trigeminal sensory afference in the SpV of the brainstem. We also noted lateralization of the DTI and PET findings, consistent with the lateralized migraine severity reported by our patient cohort. Thus, our data support a conceptually and mechanistically novel aspect of migraine pathophysiology, reflected by *in vivo* multimodal neuroimaging of the structural and functional interplay of the trigeminal system in patients suffering from migraine.

Conventional MRI of patients with migraine does not typically reveal gross brain abnormalities. In particular, while the small-scale structure of the trigeminal nerves is clearly visible on a conventional T1-weighted MRI image, such images do not differentiate patients from healthy adults, and do not elucidate the underlying pathophysiological mechanisms of migraine disease. More advanced neuroimaging techniques, such as DTI, PET, or fMRI, however, may be promising

for the objective assessment of migraine. For instance, several DTI studies have demonstrated decreased FA at the trigeminal REZ in neurological conditions such as trigeminal neuralgia[13,65–67] and temporomandibular disorder[68], though only a single, innovative study suggested such alterations in migraine.[25] Consistent with our results, Mungoven *et al.* found decreased FA in the left trigeminal REZ in migraine patients compared to healthy controls, using 3T MRI with a relatively coarse DTI resolution of 2 x 2 x 2.5 mm^3, and no further exploration of lateralization or underlying mechanisms.[25] Our study was able to achieve improved spatial resolution and ROI placement by using ultra-high field 7T MRI, and coupled multimodal imaging extended these findings to more precisely explore pathophysiology. In fact, the trigeminal nerve root may be a critical structure for assessment in migraine, as a few millimeters distal to the REZ is where the transition between the peripheral myelin and central myelin occurs[69], suggesting a potentially vulnerable site for aberrant neurochemical cross-talk. In the current study, we found a significant bilateral reduction in FA in the trigeminal REZ in migraine patients. While such changes in FA may be caused by various factors, this DTI metric is believed to be a sensitive measure of overall white matter microstructure[70], and a reduction in FA suggests damage to the nerve.[13] Furthermore, we found significantly elevated RD and MD in migraine patients on the right side. Histological studies have demonstrated that RD can detect the extent of demyelination[71,72], while MD has a possible link to underlying neuroinflammation/edema.[12] Overall, we found that migraine patients have altered trigeminal nerve REZ microstructure, which was more profound on the right side in our cohort.

A particularly novel aspect of our study is that it linked these DTI abnormalities to neuroinflammation and functional brainstem response, using PET and fMRI, respectively. Thus, our study examined, for the first time, potential pathophysiology associated with altered diffusivity in the trigeminal nerve of migraine. Specifically, we evaluated the role of trigeminal nerve REZ inflammation in migraine patients by linking DTI outcomes with integrated PET/MRI using the ligand [^{11}C]-PBR28. Since the [^{11}C]-PBR28 radioligand binds to the 18-kDa TSPO, which is upregulated in glial cells during neuroinflammatory responses[44,73,74], our imaging approach permitted the investigation of *in vivo* neuroinflammation in human pain conditions as detailed in our previous study.[54] We found a significant negative association between FA and [^{11}C]-PBR28 PET signal in the right trigeminal nerve REZ in migraine patients, further highlighted by a stronger association after computing left–right differences for both metrics. This suggests that greater

microstructural damage of the trigeminal nerve is specifically linked with greater neuroinflammation in this important anatomical region. Furthermore, we found that in migraine patients with low FA, right trigeminal REZ [^{11}C]-PBR28 PET signal was significantly elevated compared to healthy controls. This was not the case for migraine patients with normal FA, suggesting that only those individuals with moderate to severe microstructural alterations show a distinct neuroinflammatory pattern. Taken together, these findings reveal that neuroinflammation in migraine extends to the trigeminal REZ and provide new insight into the mechanisms underlying trigeminal nerve microstructural alterations. Importantly, while TSPO is commonly used as an imaging marker of central (e.g. brain) inflammation, it is also overexpressed in peripheral immune cells (e.g. macrophages, monocytes).[75,76] Thus, we propose that the elevation in PET signal observed in the REZ reflects an infiltration of immune cells into the trigeminal nerve[77]. Overall, our study contributes to the emergent body of work demonstrating evidence of neuroinflammation in human chronic pain conditions[45,54,59,78–80], including migraine.[30,31]

We also found a significant positive association between FA of the right trigeminal nerve REZ and fMRI response to trigeminal sensory afference in the right SpV in migraine patients. This linkage suggests that greater microstructural damage of the trigeminal nerve (i.e. reduced FA) leads to reduced communication of afference to a key trigeminal sensory nucleus in the brainstem (i.e. reduced SpV fMRI response). We also found increased right SpV fMRI activation in migraine patients compared to healthy controls, which suggests that migraine patients have hyperexcitable trigeminal response, in alignment with previous literature.[35,81,82] However, our finding of greater trigeminal REZ microstructural damage linked with reduced SpV fMRI response suggests that structural remodeling is a physiological coping mechanism that is protective of hyperexcitability in SpV – i.e. chronic hyperexcitability may lead to trigeminal REZ inflammation and reduced FA, in an attempt to limit communication of afference to SpV. Further research, one that is longitudinal in nature, is required to unpack the causal linkage between these findings. The involvement of SpV in fMRI studies of migraine is well-documented[34,36,37], including our own and other studies that have demonstrated altered SpV fMRI response to trigeminal sensory stimulation.[32,33] The role of the SpV in migraine pathophysiology is plausible given that the SpV primarily receives afference from Aδ and C fibers that mediate nociceptive inputs resulting in craniofacial pain sensations.[83,84] Importantly, our ultra-high field 7T fMRI acquisition (1.5 mm isotropic voxel size), combined with sophisticated co-registration techniques to project fMRI results over a high resolution (0.2

mm isotropic voxel size) brainstem underlay, enabled improved visualization and confidence in the anatomical localization of the fMRI cluster consistent with putative SpV (pars oralis) – a significant challenge for brainstem neuroimaging.

Lastly, examination of the rich clinical data collected via the daily headache diaries revealed that our predominantly right-sided DTI and PET findings may be driven by the preponderance of patients in our cohort who exhibited predominantly right-sided headache symptoms. This association was observed when considering headaches during the 30-day window prior to the PET/MRI visit and the 15-day window prior to the 7T MRI visit, respectively. Specifically, we find that migraine patients with right-dominant headaches report significantly higher migraine pain intensity compared to patients with left-dominant headaches during these windows. Differences in time windows for PET and DTI outcomes may reflect the underlying pathophysiology manifesting in neuroinflammatory versus microstructural changes seen at the trigeminal nerve REZ. These clinical findings also highlight the critical, dynamic impact migraine symptom severity and laterality may have on brain structure and function in patients with migraine.

We note several limitations to our study. First, we were limited by the comparatively lower number of healthy controls, due in part to the stringent criteria requiring healthy volunteers to complete a 4-week period of daily diaries and report no headaches characteristic of migraine. Despite this, we were able to observe significant differences in all imaging modalities between migraine patients and healthy controls. Second, the study did not include an additional control group of patients with non-migraine pain (e.g. tension-type headache or cluster headache), which would have allowed us to draw conclusions about the degree to which our findings may be specific to migraine. Third, while 7T MRI allowed for improved spatial resolution and ROI placement at the trigeminal REZ, given the small anatomy of the nerve and surrounding cerebrospinal fluid, partial volume effects may still arise with the spatial resolution used in our study (DTI = 1 x 1 x 1 mm^3 and PET = 2–3 mm). Lastly, we acknowledge that the experimenter was not blinded to participant group allocation during ROI placement but was blinded with regards to clinical characteristics (e.g., headache dominance). However, systematic bias across the large number of participants would be unlikely.

In conclusion, our multimodal DTI/PET/fMRI study conceptually and mechanistically demonstrated a novel aspect of migraine pathophysiology, reflected in the structural and functional interplay of the trigeminal system in patients suffering from migraine. Our findings are compatible

with the trigeminovascular hypothesis of migraine[85], demonstrating the fundamental role of the trigeminal nerve in this complex and difficult-to-treat neurological disorder, and supporting a linkage between peripheral and central factors. Identification of the mechanisms that contribute to migraine sensory hypersensitivity, symptom frequency, and severity can be gleaned from the peripheral and central nervous system changes that characterize migraine. Moreover, identifying this circuitry will lead to the development of novel therapies for this prevalent disorder for which trigeminal system remodeling may be an important aspect of the dynamics underlying migraine pathophysiology.

Data availability

The authors confirm that the data supporting the findings of this study are available within the article or from the corresponding author upon reasonable request.

Acknowledgements

The authors would like to thank Ellie Minhae Kim, Noreen Ward, Hannah Goodman, Grae Arabasz, Oliver Ramsay, Jonathan Polimeni, Meena Makary, and Courtney Chane for help with data collection and technical assistance. Much of the computation resources required for this research was performed on computational hardware generously provided by the Massachusetts Life Sciences Center (https://www.masslifesciences.com/).

Funding

This work was primarily supported by the National Institutes of Health, National Center for Complementary and Integrative Health (NIH NCCIH) (P01-AT009965). Further support was provided by NIH NIMH (U54-MH118919 to RG and VN), NIAMS (R01-AR079110 to MLL and VN), and NCCIH (U24-AT012560 and R01-AT011429 to VN). Support was also provided to VN by KIOM KSN2213010. ST was supported by the Canadian Institutes of Health Research Fellowship (MFE-176554) and MD was supported by NIH NCCIH (T32-AT000051).

Competing interests

VN is a paid consultant for Cala Health, a bioelectronic medicine company developing wearable neuromodulation therapies. VN's interests were reviewed and are managed by Spaulding Rehabilitation Hospital and Mass General Brigham in accordance with their conflict-of-interest policies. The rest of the authors report no competing interests.

Supplementary material

Supplementary material is available at *Brain* online.

References

1. Vos T, Abajobir AA, Abate KH, et al. Global, regional, and national incidence, prevalence, and years lived with disability for 328 diseases and injuries for 195 countries, 1990–2016: a systematic analysis for the Global Burden of Disease Study 2016. *The Lancet.* 2017;390(10100):1211-1259.

2. Headache Classification Committee of the International Headache Society (IHS). The International Classification of Headache Disorders, 3rd edition. *Cephalalgia*. 2018;38(1):1-211.

3. Pietrobon D, Moskowitz MA. Pathophysiology of migraine. *Annu Rev Physiol*. 2013;75:365-391.

4. Moskowitz MA. The neurobiology of vascular head pain. *Ann Neurol Off J Am Neurol Assoc Child Neurol Soc*. 1984;16(2):157-168.

5. Noseda R, Burstein R. Migraine pathophysiology: anatomy of the trigeminovascular pathway and associated neurological symptoms, CSD, sensitization and modulation of pain. *Pain*. 2013;154 Suppl 1:S44-53.

6. Olesen J, Burstein R, Ashina M, Tfelt-Hansen P. Origin of pain in migraine: evidence for peripheral sensitisation. *Lancet Neurol*. 2009;8(7):679-690.

7. Pietrobon D, Striessnig J. Neurobiology of migraine. *Nat Rev Neurosci*. 2003;4(5):386-398.

8. Schwedt TJ, Dodick DW. Advanced neuroimaging of migraine. *Lancet Neurol*. 2009;8(6):560-568.

9. Schmid AB, Campbell J, Hurley SA, et al. Feasibility of diffusion tensor and morphologic imaging of peripheral nerves at ultra-high field strength. *Invest Radiol*. 2018;53(12):705-713.

10. Sclocco R, Garcia RG, Kettner NW, et al. The influence of respiration on brainstem and cardiovagal response to auricular vagus nerve stimulation: A multimodal ultrahigh-field (7T) fMRI study. *Brain Stimulat*. 2019;12(4):911-921.

11. Sclocco R, Beissner F, Bianciardi M, Polimeni JR, Napadow V. Challenges and opportunities for brainstem neuroimaging with ultrahigh field MRI. *Neuroimage*. 2018;168:412-426.

12. Alexander AL, Lee JE, Lazar M, Field AS. Diffusion tensor imaging of the brain. *Neurotherapeutics*. 2007;4(3):316-329.

13. DeSouza DD, Hodaie M, Davis KD. Abnormal trigeminal nerve microstructure and brain white matter in idiopathic trigeminal neuralgia. *PAIN®*. 2014;155(1):37-44.

14. Sexton CE, Kalu UG, Filippini N, Mackay CE, Ebmeier KP. A meta-analysis of diffusion tensor imaging in mild cognitive impairment and Alzheimer's disease. *Neurobiol Aging*. 2011;32(12):2322-e5.

15. Tae WS, Ham BJ, Pyun SB, Kang SH, Kim BJ. Current clinical applications of diffusion-tensor imaging in neurological disorders. *J Clin Neurol Seoul Korea*. 2018;14(2):129.

16. Tohyama S, Walker MR, Zhang JY, Cheng JC, Hodaie M. Brainstem trigeminal fiber microstructural abnormalities are associated with treatment response across subtypes of trigeminal neuralgia. *Pain*. 2021;162(6):1790-1799.

17. Tohyama S, Hung PSP, Cheng JC, et al. Trigeminal neuralgia associated with a solitary pontine lesion: clinical and neuroimaging definition of a new syndrome. *Pain*. 2020;161(5):916-925.

18. Chong CD, Schwedt TJ. Migraine affects white-matter tract integrity: a diffusion-tensor imaging study. *Cephalalgia*. 2015;35(13):1162-1171.

19. Coppola G, Tinelli E, Lepre C, et al. Dynamic changes in thalamic microstructure of migraine without aura patients: a diffusion tensor magnetic resonance imaging study. *Eur J Neurol.* 2014;21(2):287-e13.

20. DaSilva AF, Granziera C, Tuch DS, Snyder J, Vincent M, Hadjikhani N. Interictal alterations of the trigeminal somatosensory pathway and periaqueductal gray matter in migraine. *Neuroreport.* 2007;18(4):301-305.

21. Dobos D, Kökönyei G, Gyebnár G, et al. Microstructural differences in migraine: A diffusion-tensor imaging study. *Cephalalgia*. 2023;43(12):03331024231216456.

22. Planchuelo-Gómez Á, García-Azorín D, Guerrero ÁL, Aja-Fernández S, Rodríguez M, de Luis-García R. White matter changes in chronic and episodic migraine: a diffusion tensor imaging study. *J Headache Pain*. 2020;21:1-15.

23. Rahimi R, Dolatshahi M, Abbasi-Feijani F, et al. Microstructural white matter alterations associated with migraine headaches: a systematic review of diffusion tensor imaging studies. *Brain Imaging Behav*. 2022;16(5):2375-2401.

24. Szabó N, Kincses ZT, Párdutz Á, et al. White matter microstructural alterations in migraine: a diffusion-weighted MRI study. *Pain*. 2012;153(3):651-656.

25. Mungoven TJ, Meylakh N, Marciszewski KK, Macefield VG, Macey PM, Henderson LA. Microstructural changes in the trigeminal nerve of patients with episodic migraine assessed using magnetic resonance imaging. *J Headache Pain*. 2020;21:1-11.

26. Marciszewski KK, Meylakh N, Di Pietro F, Macefield VG, Macey PM, Henderson LA. Altered brainstem anatomy in migraine. *Cephalalgia*. 2018;38(3):476-486.

27. Banati R, Myers R, Kreutzberg G. PK ('peripheral benzodiazepine')–binding sites in the CNS indicate early and discrete brain lesions: microautoradiographic detection of [3H] PK 11195 binding to activated microglia. *J Neurocytol.* 1997;26:77-82.

28. Narayan N, Owen DR, Mandhair H, et al. Translocator protein as an imaging marker of macrophage and stromal activation in rheumatoid arthritis pannus. *J Nucl Med*. 2018;59(7):1125-1132.

29. Owen DR, Narayan N, Wells L, et al. Pro-inflammatory activation of primary microglia and macrophages increases 18 kDa translocator protein expression in rodents but not humans. *J Cereb Blood Flow Metab*. 2017;37(8):2679-2690.

30. Albrecht DS, Mainero C, Ichijo E, et al. Imaging of neuroinflammation in migraine with aura: A [11C] PBR28 PET/MRI study. *Neurology*. 2019;92(17):e2038-e2050.

31. Hadjikhani N, Albrecht DS, Mainero C, et al. Extra-axial inflammatory signal in parameninges in migraine with visual aura. *Ann Neurol*. 2020;87(6):939-949.

32. Lee J, Lin RL, Garcia RG, et al. Reduced insula habituation associated with amplification of trigeminal brainstem input in migraine. *Cephalalgia*. 2017;37(11):1026-1038.

33. Stankewitz A, Aderjan D, Eippert F, May A. Trigeminal nociceptive transmission in migraineurs predicts migraine attacks. *J Neurosci*. 2011;31(6):1937-1943.

34. Borsook D, Burstein R, Moulton E, Becerra L. Functional imaging of the trigeminal system: applications to migraine pathophysiology. *Headache J Head Face Pain*. 2006;46:S32-S38.

35. Messina R, Rocca MA, Goadsby PJ, Filippi M. Insights into migraine attacks from neuroimaging. *Lancet Neurol*. Published online 2023.

36. Borsook D, Burstein R, Becerra L. Functional imaging of the human trigeminal system: opportunities for new insights into pain processing in health and disease. *J Neurobiol*. 2004;61(1):107-125.

37. Lim M, Jassar H, Kim DJ, Nascimento TD, DaSilva AF. Differential alteration of fMRI signal variability in the ascending trigeminal somatosensory and pain modulatory pathways in migraine. *J Headache Pain*. 2021;22:1-15.

38. Serrano D, Lipton RB, Scher AI, et al. Fluctuations in episodic and chronic migraine status over the course of 1 year: implications for diagnosis, treatment and clinical trial design. *J Headache Pain*. 2017;18:1-12.

39. Wells RE, O'Connell N, Pierce CR, et al. Effectiveness of mindfulness meditation vs headache education for adults with migraine: a randomized clinical trial. *JAMA Intern Med*. 2021;181(3):317-328.

40. Mareyam A, Kirsch JE, Chang Y, Madan G, Wald LL. A 64-Channel 7T array coil for accelerated brain MRI. In: Vol 764. ; 2020.

41. Owen DR, Yeo AJ, Gunn RN, et al. An 18-kDa translocator protein (TSPO) polymorphism explains differences in binding affinity of the PET radioligand PBR28. *J Cereb Blood Flow Metab*. 2012;32(1):1-5.

42. Kolb A, Wehrl HF, Hofmann M, et al. Technical performance evaluation of a human brain PET/MRI system. *Eur Radiol*. 2012;22:1776-1788.

43. Catana C, Benner T, van der Kouwe A, et al. MRI-assisted PET motion correction for neurologic studies in an integrated MR-PET scanner. *J Nucl Med*. 2011;52(1):154-161.

44. Brown AK, Fujita M, Fujimura Y, et al. Radiation dosimetry and biodistribution in monkey and man of 11C-PBR28: a PET radioligand to image inflammation. *J Nucl Med*. 2007;48(12):2072-2079.

45. Albrecht D, Kim M, Akeju O, et al. The neuroinflammatory component of negative affect in patients with chronic pain. *Mol Psychiatry*. 2021;26(3):864-874.

46. Brusaferri L, Alshelh Z, Martins D, et al. The pandemic brain: Neuroinflammation in non-infected individuals during the COVID-19 pandemic. *Brain Behav Immun*. 2022;102:89-97.

47. Gorgolewski KJ, Auer T, Calhoun VD, et al. The brain imaging data structure, a format for organizing and describing outputs of neuroimaging experiments. *Sci Data*. 2016;3(1):1-9.

48. Jenkinson, M., Beckmann, C.F., Behrens, T.E., Woolrich, M.W., Smith, S.M., 2012. FSL. Neuroimage 62, 782–790.

49. Andersson JL, Skare S, Ashburner J. How to correct susceptibility distortions in spin-echo echo-planar images: application to diffusion tensor imaging. *Neuroimage*. 2003;20(2):870-888.

50. Andersson JL, Graham MS, Zsoldos E, Sotiropoulos SN. Incorporating outlier detection and replacement into a non-parametric framework for movement and distortion correction of diffusion MR images. *Neuroimage*. 2016;141:556-572.

51. Andersson JL, Sotiropoulos SN. An integrated approach to correction for off-resonance effects and subject movement in diffusion MR imaging. *Neuroimage*. 2016;125:1063-1078.

52. Behrens TE, Woolrich MW, Jenkinson M, et al. Characterization and propagation of uncertainty in diffusion-weighted MR imaging. *Magn Reson Med Off J Int Soc Magn Reson Med*. 2003;50(5):1077-1088.

53. Izquierdo-Garcia D, Hansen AE, Förster S, et al. An SPM8-based approach for attenuation correction combining segmentation and nonrigid template formation: application to simultaneous PET/MR brain imaging. *J Nucl Med*. 2014;55(11):1825-1830.

54. Loggia ML, Chonde DB, Akeju O, et al. Evidence for brain glial activation in chronic pain patients. *Brain*. 2015;138(3):604-615.

55. Ashburner J, Friston KJ. Unified segmentation. *Neuroimage*. 2005;26(3):839-851.

56. Zaretskaya N, Fischl B, Reuter M, Renvall V, Polimeni JR. Advantages of cortical surface reconstruction using submillimeter 7 T MEMPRAGE. *Neuroimage*. 2018;165:11-26.

57. Esteban O, Markiewicz CJ, Blair RW, et al. fMRIPrep: a robust preprocessing pipeline for functional MRI. *Nat Methods*. 2019;16(1):111-116.

58. Fedorov A, Beichel R, Kalpathy-Cramer J, et al. 3D Slicer as an image computing platform for the Quantitative Imaging Network. *Magn Reson Imaging*. 2012;30(9):1323-1341.

59. Sandström A, Torrado-Carvajal A, Morrissey EJ, et al. [11C]-PBR28 positron emission tomography signal as an imaging marker of joint inflammation in knee osteoarthritis. *PAIN*. 2024;165(5). https://journals.lww.com/pain/fulltext/2024/05000/_11c__pbr28_positron_emission_tomography_signal_as.19.aspx

60. Avants BB, Tustison NJ, Song G, Cook PA, Klein A, Gee JC. A reproducible evaluation of ANTs similarity metric performance in brain image registration. *Neuroimage*. 2011;54(3):2033-2044.

61. Woolrich MW, Ripley BD, Brady M, Smith SM. Temporal autocorrelation in univariate linear modeling of FMRI data. *Neuroimage*. 2001;14(6):1370-1386.

62. Woolrich MW, Behrens TE, Beckmann CF, Jenkinson M, Smith SM. Multilevel linear modelling for FMRI group analysis using Bayesian inference. *Neuroimage*. 2004;21(4):1732-1747.

63. Naidich TP, Duvernoy HM, Delman BN, Sorensen AG, Kollias SS, Haacke EM. *Duvernoy's Atlas of the Human Brain Stem and Cerebellum: High-Field MRI, Surface Anatomy, Internal Structure, Vascularization and 3 D Sectional Anatomy*. Springer Science & Business Media; 2009.

64. Calabrese E, Hickey P, Hulette C, et al. Postmortem diffusion MRI of the human brainstem and thalamus for deep brain stimulator electrode localization. *Hum Brain Mapp*. 2015;36(8):3167-3178.

65. Herweh C, Kress B, Rasche D, et al. Loss of anisotropy in trigeminal neuralgia revealed by diffusion tensor imaging. *Neurology*. 2007;68(10):776-778.

66. Leal PRL, Roch JA, Hermier M, Souza MAN, Cristino-Filho G, Sindou M. Structural abnormalities of the trigeminal root revealed by diffusion tensor imaging in patients with trigeminal neuralgia caused by neurovascular compression: a prospective, double-blind, controlled study. *Pain*. 2011;152(10):2357-2364.

67. Lutz J, Linn J, Mehrkens JH, et al. Trigeminal neuralgia due to neurovascular compression: high-spatial-resolution diffusion-tensor imaging reveals microstructural neural changes. *Radiology*. 2011;258(2):524-530.

68. Moayedi M, Weissman-Fogel I, Salomons TV, et al. White matter brain and trigeminal nerve abnormalities in temporomandibular disorder. *PAIN®*. 2012;153(7):1467-1477.

69. Peker S, Kurtkaya Ö, Üzün İ, Pamir MN. Microanatomy of the central myelin-peripheral myelin transition zone of the trigeminal nerve. *Neurosurgery*. 2006;59(2):354-359.

70. O'Donnell LJ, Westin CF. An introduction to diffusion tensor image analysis. *Neurosurg Clin*. 2011;22(2):185-196.

71. Song SK, Yoshino J, Le TQ, et al. Demyelination increases radial diffusivity in corpus callosum of mouse brain. *Neuroimage*. 2005;26(1):132-140.

72. Song SK, Sun SW, Ramsbottom MJ, Chang C, Russell J, Cross AH. Dysmyelination revealed through MRI as increased radial (but unchanged axial) diffusion of water. *Neuroimage*. 2002;17(3):1429-1436.

73. Lavisse S, Guillermier M, Hérard AS, et al. Reactive astrocytes overexpress TSPO and are detected by TSPO positron emission tomography imaging. *J Neurosci*. 2012;32(32):10809-10818.

74. Papadopoulos V, Baraldi M, Guilarte TR, et al. Translocator protein (18 kDa): new nomenclature for the peripheral-type benzodiazepine receptor based on its structure and molecular function. *Trends Pharmacol Sci*. 2006;27(8):402-409.

75. Cosenza-Nashat M, Zhao M, Suh H, et al. Expression of the translocator protein of 18 kDa by microglia, macrophages and astrocytes based on immunohistochemical localization in abnormal human brain. *Neuropathol Appl Neurobiol*. 2009;35(3):306-328.

76. Lacor P, Benavides J, Ferzaz B. Enhanced expression of the peripheral benzodiazepine receptor (PBR) and its endogenous ligand octadecaneuropeptide (ODN) in the regenerating adult rat sciatic nerve. *Neurosci Lett*. 1996;220(1):61-65.

77. Franceschini A, Vilotti S, Ferrari MD, Van Den Maagdenberg AM, Nistri A, Fabbretti E. TNFα levels and macrophages expression reflect an inflammatory potential of trigeminal ganglia in a mouse model of familial hemiplegic migraine. *PloS One*. 2013;8(1):e52394.

78. Albrecht DS, Ahmed SU, Kettner NW, et al. Neuroinflammation of the spinal cord and nerve roots in chronic radicular pain patients. *Pain*. 2018;159(5):968-977.

79. Alshelh Z, Brusaferri L, Saha A, et al. Neuroimmune signatures in chronic low back pain subtypes. *Brain*. 2022;145(3):1098-1110.

80. Brusaferri L, Alshelh Z, Schnieders JH, et al. Neuroimmune activation and increased brain aging in chronic pain patients after the COVID-19 pandemic onset. *Brain Behav Immun*. 2024;116:259-266.

81. Katsarava Z, Lehnerdt G, Duda B, Ellrich J, Diener H, Kaube H. Sensitization of trigeminal nociception specific for migraine but not pain of sinusitis. *Neurology*. 2002;59(9):1450-1453.

82. Maleki N, Szabo E, Becerra L, et al. Ictal and interictal brain activation in episodic migraine: neural basis for extent of allodynia. *PloS One*. 2021;16(1):e0244320.

83. Dostrovsky JO. Brainstem and thalamic relays. In: *Handbook of Clinical Neurology*. Vol 81. Elsevier; 2006:127-139.

84. Sessle BJ. Acute and chronic craniofacial pain: brainstem mechanisms of nociceptive transmission and neuroplasticity, and their clinical correlates. *Crit Rev Oral Biol Med*. 2000;11(1):57-91.

85. Ashina M, Hansen JM, Do TP, Melo-Carrillo A, Burstein R, Moskowitz MA. Migraine and the trigeminovascular system—40 years and counting. *Lancet Neurol*. 2019;18(8):795-804.

Figure Legends

Figure 1 White matter microstructural alterations in trigeminal nerve of migraine patients. **(A)** Representative example of a T1-weighted MP-RAGE anatomical image in the axial view at the mid-pontine level of the brainstem. Blue box depicts the magnified area of the pons and trigeminal nerves with region-of-interest placement at the right and left trigeminal REZ (shown in red, 4 voxels in size). **(B and C)** Bar graphs illustrating average DTI metrics (FA, RD, MD, and AD) ± SEM of migraine patients (red) and healthy controls (blue) for the right (B) and left (C) trigeminal REZ. Migraine patients exhibit significant microstructural alterations in the trigeminal REZ as characterized by lower FA (right and left side), higher RD (right only), and higher MD (right only) compared to healthy controls. * = $p < 0.05$, ** = $p < 0.01$, **** = $p < 0.0001$ (FDR-corrected). AD, axial diffusivity; FA, fractional anisotropy; HC, healthy controls; MD, mean diffusivity; MIG, migraine patients; RD, radial diffusivity.

Figure 2 Combining DTI and PET: Association between trigeminal nerve microstructure and neuroinflammation in migraine patients. **(A)** Representative example of a trigeminal REZ [^{11}C]-PBR28 PET SUVR map and corresponding T1-weighted image in the axial view in a migraine patient. **(B)** Scatterplots illustrating the relationship between [^{11}C]-PBR28 PET signal and FA in the right and left trigeminal REZ, as well as the difference (left–right) in the migraine

patient group only. Significant negative associations were found on the right side and the Δ. SUVR and FA values are adjusted for TSPO polymorphism. **(C)** Bar graphs illustrating average PET signal ± SEM of migraine patients with low FA (closed red circles), high FA (open red circles) and healthy controls (blue) for the right and left trigeminal REZ. The right side shows a significant group effect, driven by patients with low FA with elevated PET signal compared to healthy controls. ** = $p < 0.01$ (post-hoc Dunnett's test comparing each patient subgroup against a single healthy control group). FA, fractional anisotropy; HC, healthy controls; HFA, high fractional anisotropy; LFA, low fractional anisotropy; MIG, migraine patients; REZ, root entry zone; SUVR, standardized uptake value ratio.

Figure 3 Combining DTI and fMRI: Association between trigeminal nerve microstructure and brainstem functional response to trigeminal sensory afference in migraine patients. (A) Schematic of the positioning of the non-painful electrical forehead stimulation targeting the right trigeminal nerve territory and the block fMRI design used (stimulus comes ON for 8 seconds and turns OFF for 14 seconds for a total of 17 stimulations). **(B)** Result from the voxelwise analysis showing the right SpV cluster, overlaid on a high resolution 0.2 mm *ex vivo* B_0 brainstem, where fMRI response to trigeminal sensory stimulation on the right side is significantly positively associated with FA of the right trigeminal REZ in the migraine patient group. The Duvernoy's brainstem atlas slice shown aided the anatomical localization of the SpV (pars oralis) fMRI response. FA, fractional anisotropy; REZ, root entry zone. r = regression coefficient from General Linear Model analysis in FSL.

Table 1 Demographic and clinical characteristics of study participants

	Migraine patients (n=60)	Healthy controls (n=20)
Age, mean in years (SD)	36.3 (12.0)	35.5 (13.3)
Sex, n (%)		
Female	55 (92)	19 (95)
Male	5 (8)	1 (5)
Gender, n (%)		
Woman	53 (89)	19 (95)
Man	5 (8)	1 (5)
Non-binary	2 (3)	0 (0)
Race, n (%)		
White	52 (87)	10 (50)
Black	4 (6)	1 (5)
Asian	3 (5)	6 (30)
Other	1 (2)	3 (15)
Migraine Characteristics		
Headache Frequency[a], mean (SD, range)	9.5 (4.0, 4-20)	n/a
Pain Intensity[b], mean (SD, range)	4.3 (1.3, 1.8–7.4)	n/a
Disease Duration[c], mean (SD, range)	16.9 (10.5, 3–48)	n/a
Migraine with Aura, n (%)	19 (32)	n/a
Migraine Medication, n (%)		
Preventive[d]	28 (47)	n/a
Acute[e]	59 (98)	n/a
Both	27 (45)	n/a

[a]Average number of attacks during four weeks of daily diary completion.
[b]Average headache pain intensity (0-10) during four weeks of daily diary completion.
[c]Average of the total years that participants have experienced migraines.
[d]Preventive medications: Amitriptyline, Baclofen, CGRPmAb, Metoprolol, Nortriptylin, OnabotulinumtoxinA, Pregabalin, Propranolol, Topiramate, Tizanidine, Valproate, Venlafaxine.
[e]Acute medications: Acetaminophen, Benadryl, Butalbital, Caffeine, Cyclobenzaprine, NSAIDs, Triptans, Ubrogepan.

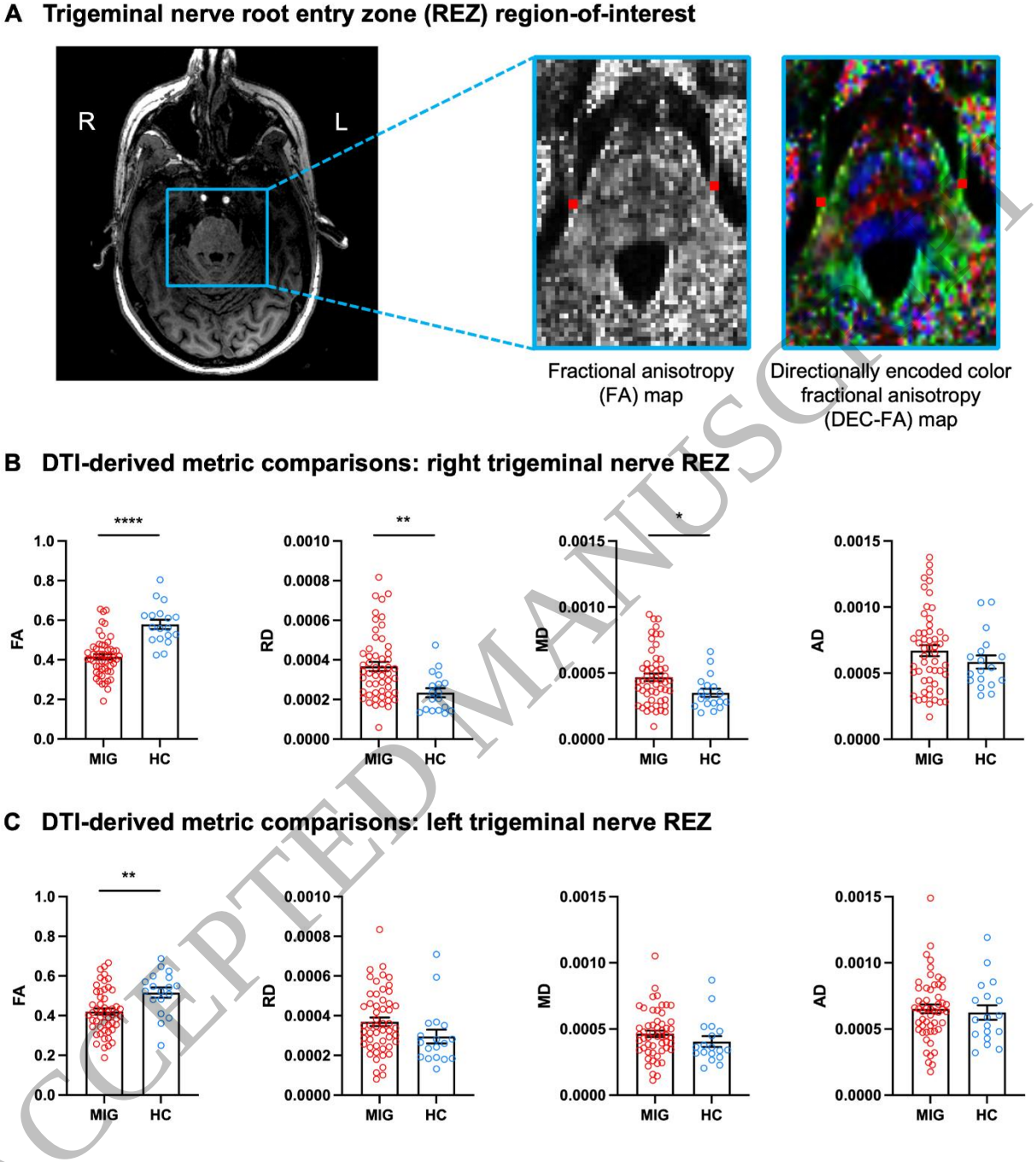

Figure 1
186x204 mm (DPI)

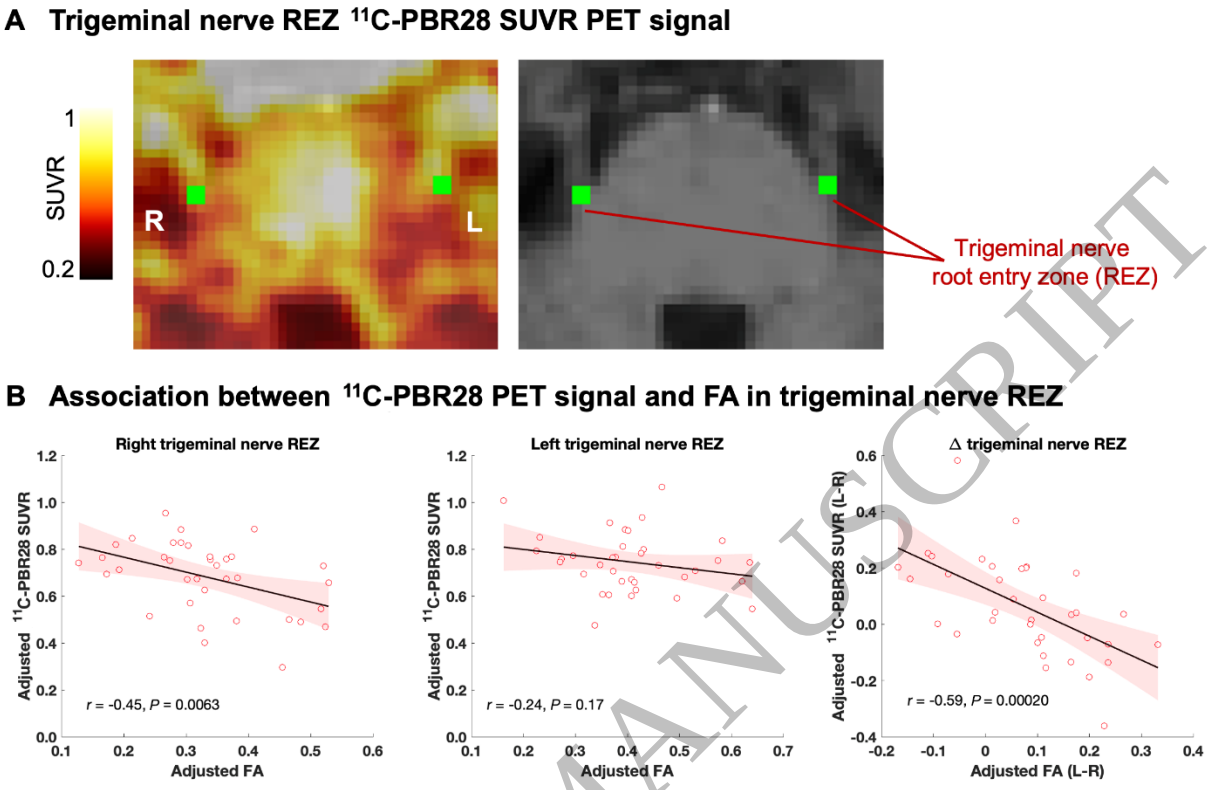

Figure 2
205x199 mm (DPI)

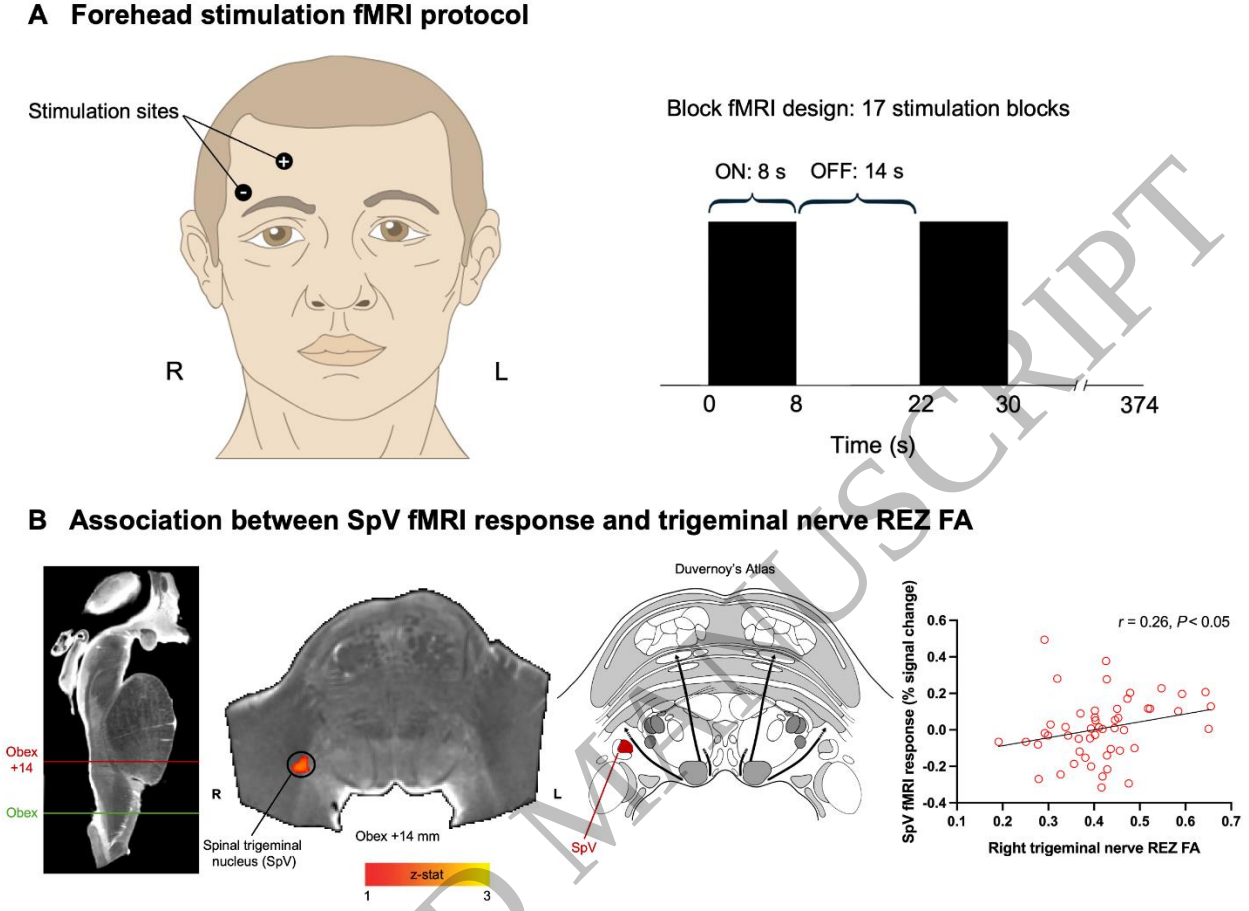

Figure 3
194x150 mm (DPI)